GeoScienceWorld
Lithosphere
Volume 2022, Article ID 5447973, 14 pages
https://doi.org/10.2113/2022/5447973

Lithosphere

Research Article

Experimental Study on Damage Characteristics of Coal Samples under True Triaxial Loading and Dynamic Unloading

Anye Cao,[1,2,3] Changbin Wang,[4] Ning Zhang,[1] Hui Li,[1] Zhigang Liu,[1,5,6] and Sheng Zhi[7]

[1]*School of Mines, China University of Mining and Technology, Xuzhou 221116, China*
[2]*Jiangsu Engineering Laboratory of Mine Earthquake Monitoring and Prevention, China University of Mining and Technology, Xuzhou 221116, China*
[3]*Xuzhou Wushuo Information Co., Ltd., Xuzhou, Jiangsu 221116, China*
[4]*State Key Laboratory of Coal Resources and Safe Mining, China University of Mining & Technology, Xuzhou, Jiangsu 221116, China*
[5]*Institute of Mining Engineering, Shandong University of Science and Technology, Tai'an 271019, China*
[6]*Shandong Energy Group, Jinan 250013, China*
[7]*Department of Risk Management, China Huarong International Holdings Limited, China*

Correspondence should be addressed to Changbin Wang; changbin.wang@cumt.edu.cn

Received 24 June 2022; Accepted 12 August 2022; Published 29 August 2022

Academic Editor: Guangyao Si

Coal bursts are one of the formidable hazards in underground coal mines, yet it is still not fully explored due to the complex stress environment that exists during mining. To better understand the bursting mechanism of coal under real-time mining conditions, it is necessary to develop an experimental method capable of reproducing in situ stress and loading-unloading paths of coal in in situ conditions. In this study, a self-developed true triaxial testing system was used to investigate the damage and failure characteristics of coal samples under true triaxial loading and dynamic unloading conditions. Acoustic Emission (AE) monitoring was used to capture the fracturing of the loaded coal. Passive Velocity Tomography (*PVT*) and Cumulative AE Energy Density (*CAEED*) were used to analyse damage evolution characteristics of the coal samples under true triaxial loading conditions. A high-speed camera was used to record the failure of the coal samples when the minimum principal stress σ_3 was suddenly unloaded. It was found that continuous coal damage occurred primarily during the true triaxial loading period. The peak number of AE events in the coal samples increased and then dropped as σ_1 levels increased. High and low wave velocity zones in the coal samples represent regenerations of the high-density zone and fracture emergence, respectively. Significant energy release zones transferred and expanded as the triaxial loading level increased. Under significant triaxial loads, the coal samples failed and were severely damaged, and the dynamic unloading of σ_3 caused ejections of coal fragments at low velocities. The outcome of this study provides in-depth understanding of the failure mechanism of coal under in situ conditions.

1. Introduction

Rockbursts are one of the most formidable hazards in underground mining. It is defined as the dynamic failure of rock mass accompanied by an instant energy release, which causes violent fragment ejection into the excavations [1, 2]. When this phenomenon occurs in a coal mine, it is typically referred to as a "coal burst" [2]. With the huge coal demand for the increasing global energy consumption in recent decades, more intensive coal extractions are carried out at greater depths. Deep coal and rock mass present a complicated geological environment with high in situ stress, where the dynamic failure of coal and rock mass is frequently triggered by large-scale mining activities [3, 4]. Coal bursts have been documented in major mining countries, including China, Australia, the United States, Poland, India, and South Africa, resulting in a large number of fatalities and economic losses [5–7]. However, even after more than a half-century

of extensive investigation, the mechanism of coal and rockbursts is still not entirely understood due to many contributing factors and uncertainties [8].

The strength and failure modes of the coal and rock mass are directly related to the in situ stress conditions, which is one of the main factors controlling the burst proneness [9]. Unexpected coal and rockbursts frequently occur near the tectonics where in situ stresses are highly anisotropic. Commonly, there are two in situ stress conditions in mines: (1) triaxial compression away from the excavation surface with $\sigma_1 \neq 0$ (the maximum principal stress), $\sigma_2 \neq 0$ (the intermediate principal stress), and $\sigma_3 \neq 0$ (the minimum principal stress) and (2) biaxial compression on the excavation surface with $\sigma_1 \neq 0$, $\sigma_2 \neq 0$, and $\sigma_3 = 0$ [10, 11]. True-triaxial loading systems have been developed in laboratories to replicate such polyaxial stress conditions of rocks [12, 13]. The mechanical characteristics and internal damage of true triaxial loaded rocks have been extensively studied using Acoustic Emission (AE) technology and numerical analysis. AE technology makes use of seismic waves emitted from the fractures in the coal and rock samples to locate internal damage and understand the failure mechanism. It was found that the rock strength usually experiences an increase and a subsequent decrease with the σ_2 increase [14, 15]. Tibbo [16] found that the differential stress $(\sigma_1 - \sigma_3)$ is the critical factor to initiate rock damage under a true triaxial compression. Haimson and Chang [14] stated that the increase of σ_2 can expand the elastic range of rocks, which is characterised by a higher onset of dilatancy relative to the σ_1 at failure. Based on the experimental results, several failure criteria have been also developed to estimate rock strength in triaxial compressing conditions, such as Mogi criterion [17], Mogi–Coulomb criterion [18], and Drucker-Prager criterion [19]. However, compared to the rocks, limited investigations have been conducted on the damage characteristics of coal under true triaxial loading conditions. Since coal has many joints and cleats, its mechanical properties greatly vary as compared to that of rocks, which makes it challenging to analyse its damage characteristics [20]. Some research work has been conducted on triaxial loaded coal, such as its strength with varying σ_2 [21], brittleness and AE energy [22], fractal dimensions of AE signals, and permeabilities for water and methane [23, 24]. Considering the significance of the anisotropic stress environment in triggering coal burst hazards, a further study is required to understand coal behaviours in different triaxial stress conditions.

Apart from the in situ stress conditions, dynamic impacts are also an important factor involved in the initiation of coal and rock bursts. It refers to the transient stress change during mining activities that can trigger violent rock failure when under critical conditions [20, 25]. Dynamic unloading during the mineral extraction is a major source of dynamic impacts in mines, which can suddenly reduce the coal and rock strength near the excavation surface and induce burst hazards [10]. Experiments have been conducted extensively to examine the dynamic unloading-related rockburst mechanism. Many researchers have successfully simulated the dynamic unloading of the rock samples by dropping a loading bar(s) in the true triaxial loading system [26, 27]. He et al. [28] and Su et al. [13] found that an anomalous time-dependent fractal dimension and specific frequency spectrum characteristics were presented prior to rockbursts. He et al. [29] observed higher amplitude and lower frequency AE events before the bursting failure, and a dramatic increase in energy release was detected during the unloading process. However, the research on the dynamic unloading to coal is still in its early stages. Previous works mostly focused on coal under conventional triaxial or biaxial compressions with regular or cycling loading [30]. Hence, to gain a deeper understanding of the coal burst mechanism under in situ conditions, it is necessary to conduct experimental tests of dynamic unloading effect on coal under true triaxial compression.

In this paper, an experimental study was conducted on the coal damage characteristics under varying true triaxial loads and dynamic unloads. The study was conducted using a modified true triaxial testing system that can simulate in situ loading and dynamic unloading paths of the cubic rock/coal sample and monitor the AE signals during the whole testing process [31]. The characteristics of time-varying stresses, total strain, and number of AE events of the coal samples under different levels of true triaxial loadings were investigated. Passive Velocity Tomography (*PVT*) and Cumulative AE Energy Density (*CAEED*) techniques were adopted to study the stress and damage evolution characteristics of coal during the triaxial loading and load holding periods. The failure mode of the triaxial loaded coal samples after suddenly unloading σ_3 was analysed by using a high-speed camera.

2. Experimental Technology and Procedure

2.1. True Triaxial Coal-Rock Dynamic Behaviour Testing System (TTCDBTS). The true triaxial coal-rock dynamic behaviour testing system (TTCDBTS) was self-developed by the China University of Mining and Technology. TTCDBTS is a multifunctional coal burst testing system designed for conducting static and/or dynamic experiments, including triaxial loading test, dynamic loading test, and unloading test. It has a servo-controlled true triaxial loading part, a sample fixture cell, a Split-Hopkinson-Pressure-Bar (SHPB) part, and a single face unloading part (see Figure 1). TTCDBTS can apply independent loads in the three principal stress directions to the sample fixture cell via six servo-controlled hydraulic pumps. The sample fixture cell was made up of six loading plates, which were used to fix the cubic sample and transmit the loads from the testing system. Six strain gauges were installed on the loading plates to measure the strain of the sample during the testing procedure. To simulate the dynamic unloading effect during the mining process, a droppable loading bar was built between the sample fixture cell and a horizontal pump, which can implement a sudden release of the minimum principal stress (σ_3) at one face of the cubic sample (see Figure 1(b)). Furthermore, TTCDBTS can conduct dynamic loading tests by using the SHPB part, which can transmit one-dimensional waves to the samples through a long elastic bar.

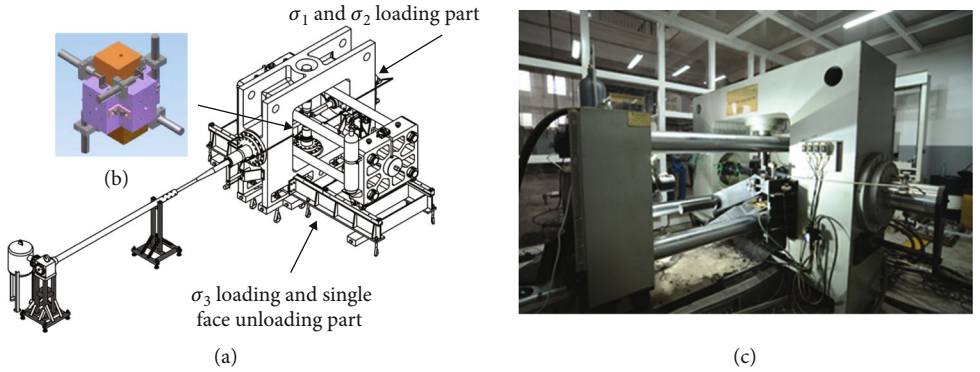

Figure 1: (a) True triaxial coal-rock dynamic behaviour testing system (TTCDBTS), (b) sample fixture cell, which is also shown in Figure 3, and (c) single face unloading part with a droppable loading bar.

2.2. Coal Samples. The coal samples for the present investigation were taken from the 5# coal seam of the Huating Coal Mine in Gansu Province, China. The average uniaxial compression strength (UCS) of the test coal was found to be 13.7 MPa. All the coal samples were cut into cubes from the coal blocks. The dimensions of the coal sample were 50 mm in width, 50 mm in length, and 100 mm in height. Huating Coal Mine is a typical burst-prone mine, which has experienced frequent coal burst hazards due to its complex geological environments and unfavourable mining conditions. The seismic monitoring system at this mine has recorded more than 200 coal bursts since 2008. The largest coal burst event that the local seismic monitoring system has recorded had seismic energy of 28.6 MJ, which caused roadway damage of tens of meters and support failure. The coal mine is prone to severe tectonic stress due to the presence of the fold structure in the coalfield. According to the geostress measurements, the average maximum principal stress (σ_1) was 25.788 MPa in the horizon, the average intermediate principal stress (σ_2) was 17.502 MPa in vertical, and the average minimum principal stress (σ_3) was 15.496 MPa. Therefore, the significant horizontal stress in this mine dominates the in situ stress, which is roughly 1.5 times the vertical stress [31]. The target #5 coal seam has a depth of 550 to 800 m, a deep angle between 1° and 15°, and an average thickness of about 40 m. Such an extremely thick coal seam was designed to be extracted in three layers, and the longwall top coal caving method was used for each 13 m thick layer (see Figure 2). Additionally, the "gob-side entry driving" (GED) method was used in the mine [32], to increase the coal recovery ratio. Herein, narrow coal pillars with widths of only 10 m or less were left between longwalls in the same layer. Intensive coal extractions and unfavourable mining methods can contribute to significantly high stresses in the coal and rock mass. Under such conditions, the dynamic loading and unloading disturbance during the mining process can easily trigger coal burst damage near the excavation.

2.3. AE Monitoring. The AE signals from the tested coal samples were successively collected using the PCI-2 AE acquisition equipment, manufactured by the Physical Acoustics Corporation (PAC). The system included a built-in waveform processing module, a filter circuit, a preamplifier, an A/D conversion module, and a computer. The maximum sampling rate of the system was 40 MSPS, and the PDT, HDT, and HLT were set as 50 μs, 200 μs, and 300 μs, respectively. AE sensors were produced by PAC with frequency ranges of 100~400 kHz. Their spatial layout around the sample is shown in Figure 3(a). Two AE sensors were placed in the centre of the top and bottom faces of the sample, respectively. The remaining six AE sensors were placed on the three side faces of the sample, with two sensors arranged diagonally on each side face. No AE sensor was placed on the side face to be loaded by the droppable loading bar, which is marked dotted face in Figure 3(a). A total of eight AE sensors were embedded in the loading plates of the sample fixture cell to achieve continuous AE monitoring

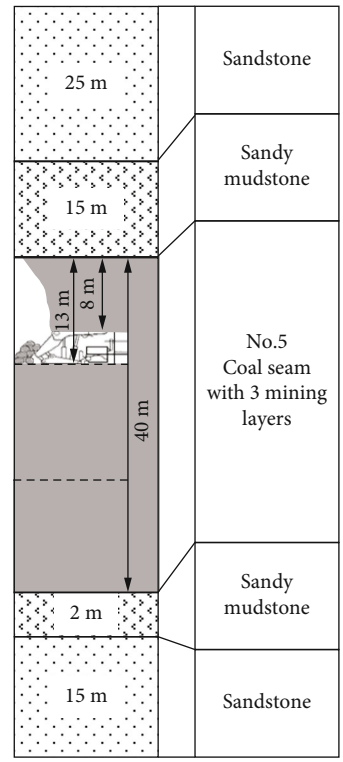

Figure 2: Typical stratigraphic column in Huating Coal Mine.

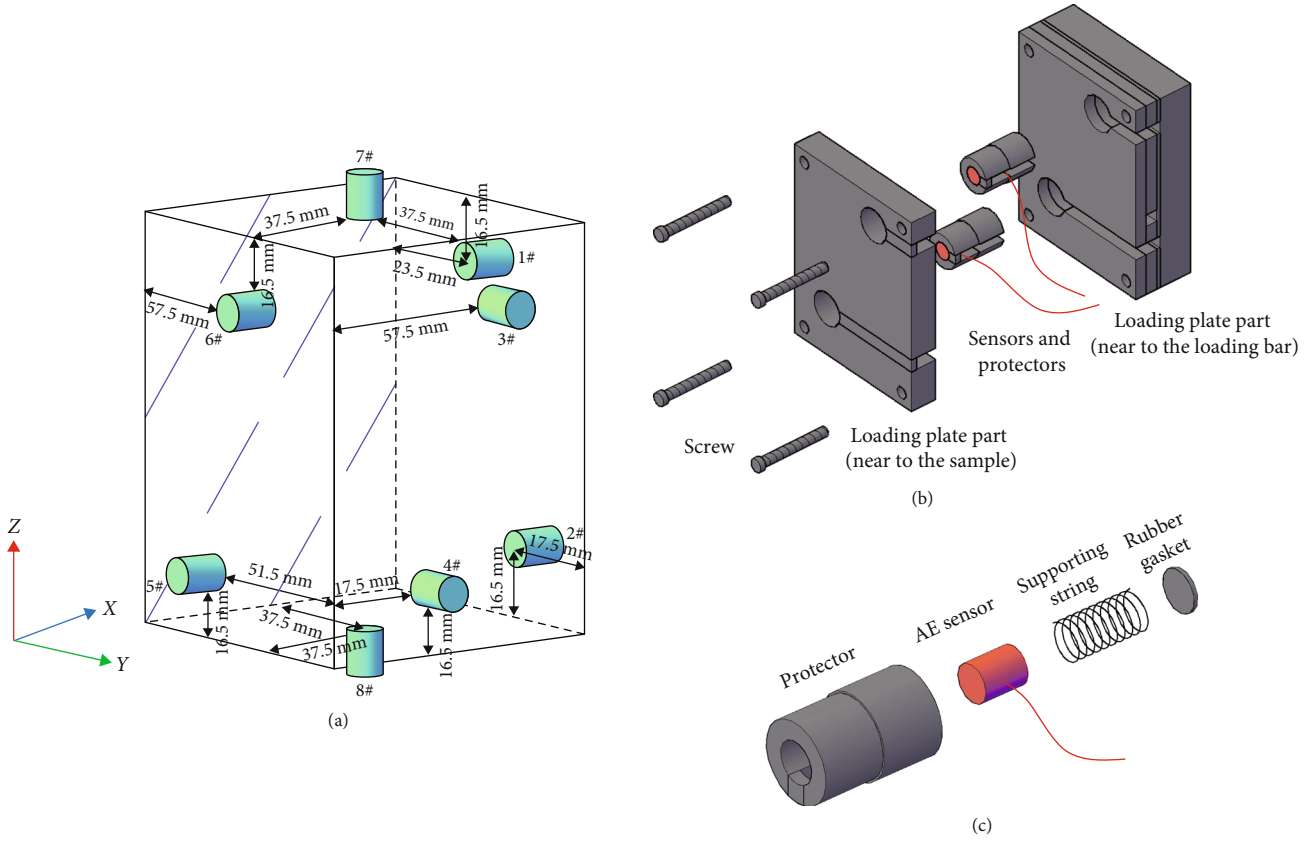

Figure 3: (a) AE sensor layout around the sample. The dotted-lined face is the one for unloading purposes. (b) Components of one side loading plate with two AE sensors. (c) An AE sensor adaptor and its inner components.

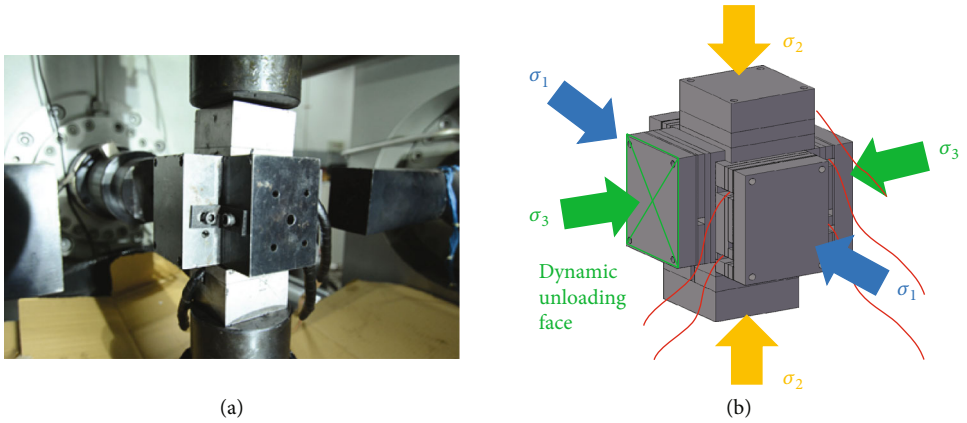

Figure 4: (a) Schematic diagram of the sample fixture cell loaded from the X (horizontal), Y (horizontal), and Z (vertical) directions. (b) The actual sample fixture cell with a sample inside in TTCDBTS.

during the triaxial loading operation, which is shown in Figure 3(b). Each AE sensor was fixed and protected by a sensor adaptor, which can be replaced to fit sensors of different sizes. A rubber pad and a string were placed on the back of the sensor in the adaptor to provide a tight attachment between the sensor and the sample surface in order to get clear acoustic waves from the loaded sample (see Figure 3(c)).

2.4. Testing Procedure. Six tests with different stress paths were carried out to replicate the in situ triaxial loading and unloading conditions of the coal mass in the Huating Coal Mine. The coal sample was cut into cubes with dimensions of 50 mm (width) × 50 mm (length) × 100 mm (height) and installed in the sample fixture cell (see Figure 4(a)). TTCDBTS applied loads from three orthogonal directions on the coal sample (see Figure 4(b)): the maximum principal

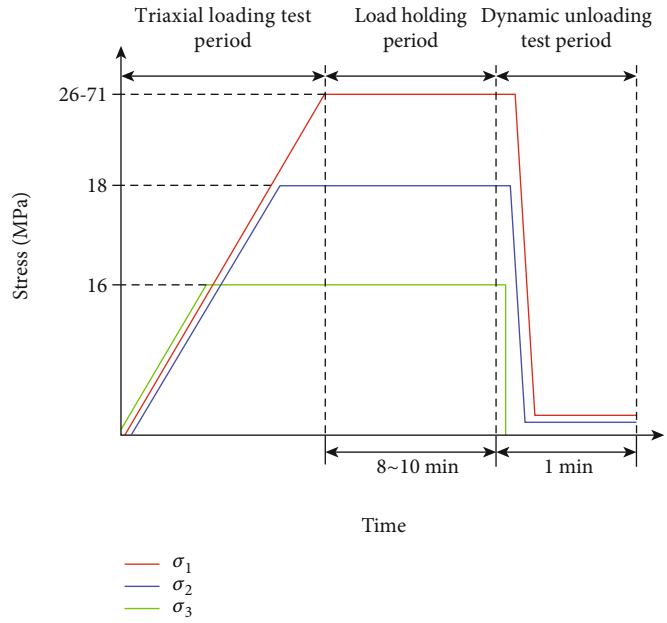

Figure 5: Loading paths of triaxial loading tests and dynamic unloading tests.

stress in the horizontal direction (σ_1), the intermediate principal stress in vertical direction(σ_2), and the minimum principal stress in horizontal direction(σ_3). To investigate the influence of high tectonic stresses on the damage in coal, σ_1 for the six tests were set as 26 MPa, 31 MPa, 36 MPa, 41 MPa, 46 MPa, and 71 MPa, respectively. According to the measured average in situ principal stresses in Section 2.2, σ_2 and σ_3 were set as 18 MPa and 16 MPa, respectively. The testing procedure was divided into three periods: triaxial loading test period, load-holding period, and dynamic unloading test period, which are explained in Figure 5. In the triaxial loading test period, the loads in all directions were firstly increased to 16 MPa. Then, σ_3 was kept as 16 MPa, while σ_1 and σ_2 increased to 18 MPa. Finally, the loads in the X direction were increased to the expected σ_1, and the loads in the Y and Z directions were kept as σ_3 and σ_2, respectively. The loading rate during the triaxial loading test period was maintained between 2×10^{-5} mm/s and 5×10^{-5} mm/s. Following the triaxial loading test period, the loads in the three directions were kept constant for about 8-10 minutes. In the dynamic unloading test period, σ_3 applied by the droppable loading bar was suddenly released and one sample face was exposed (see Figure 4(b)), while σ_1 and σ_2 were kept constant for 1 minute. The coal sample exhibited dynamic failure with fragment ejections due to the dynamic unloading of σ_3, which was captured by the high-speed camera.

3. Methodology of Damage Assessment in True Triaxially Loaded Coal Samples

3.1. Passive Velocity Tomography (PVT). The internal damage evolutions and stress conditions of the triaxially loaded coal sample were characterised using the *PVT* technology. *PVT* can inversely calculate the P-wave velocity field inside the rocks by using the AE events location and first arrival times of seismic waves. *PVT* is an ideal tool for quantifying stress levels and damage characteristics in coal and rock mass because it presents an exponential relationship between the stress applied to the rock and the P-wave velocity [4]. Suppose that the i^{th} seismic wave has the ray path L_i in the sample and the travel time T_i from the source to the sensor, the relationship between L_i and T_i can be described as

$$T_i = \int_{L_i} \frac{dL}{V(x,y,z)} = \int_{L_i} S(x,y,z)dL, \tag{1}$$

where $V(x,y,z)$ is the wave velocity along the ray path at a point and $S(x,y,z)$ is the slowness of the seismic wave. Considering that the wave ray path is commonly non-straight due to the high heterogeneity of the material, the velocity inversion can be computed by discretising the coal sample into m voxels. Therefore, T_i can also be expressed as

$$T_i = \sum_{j=1}^{m} d_{ij} S_j, \tag{2}$$

where d_{ij} is the ray length of the i^{th} seismic wave in the j^{th} voxel, and S_j is the slowness of the j^{th} voxel. d_{ij} equates to zero if the ray does not pass the voxel. The unknown ray paths of seismic waves and slowness in the grids can be derived by back calculating the matrix of slowness **S**, ray lengths in voxels **D,** and travelling times **T** for n ray paths in the sample (matrix size = $n \times m$):

$$\mathbf{T} = \mathbf{DS} \longrightarrow \mathbf{S} = \mathbf{D}^{-1}\mathbf{T}. \tag{3}$$

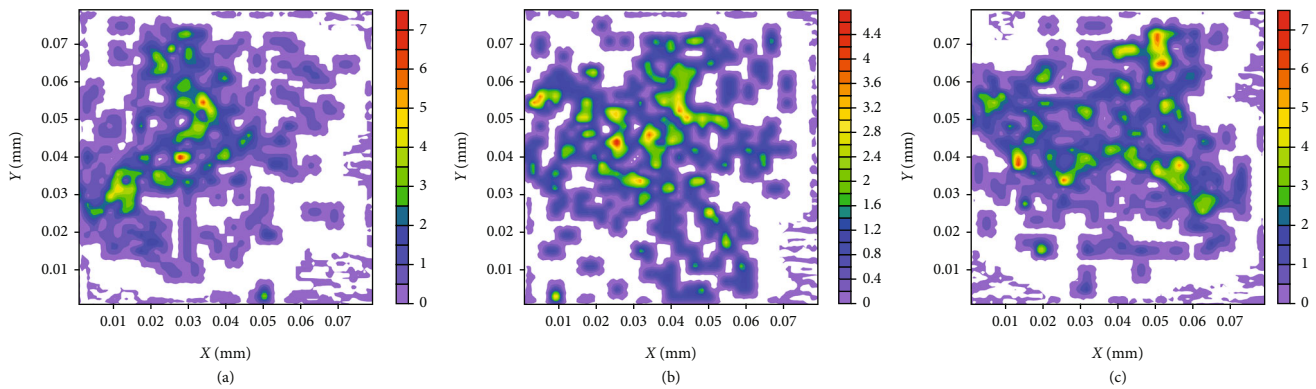

Figure 6: Example of ray density in the horizontal slices at $Z = 30$ mm (a), 50 mm (b), and 70 mm (c).

Because of the highly anisotropic distribution of ray paths in the voxels, the matrix in Equation (3) was solved using the Simultaneous Iterative Reconstructive Technique (SIRT) [33]. SIRT is an iterative method for ray tracing that minimizes the residual time for rays by adjusting the ray distances in voxels through which the rays pass. In this study, the tested coal samples were divided into voxels with dimensions of $5 \times 5 \times 5$ mm for PVT calculation.

The *PVT* performance of characterising damage evolution of the loaded sample was controlled by the number of AE events used for calculation. A larger density and coverage rate of ray paths in the sample were produced by *PVT* calculations employing more AE events, which led to a more accurate result. However, if more AE events need to be collected over a longer period of time, the *PVT* result may not be as timely and may not accurately reflect the damage evolution of coal samples during the loading process. To ensure both the accuracy and timeliness of the *PVT* results, AE events with numbers between 100 and 400 were used for each *PVT* calculating cycle in this study. Figure 6 shows ray density distribution using 100 AE events at three horizontal slices at $Z = 30$ mm, 50 mm, and 70 mm in a coal sample for example. From Figure 6, it can be observed that the ray paths from 100 AE events covered most of the area of the slices, indicating a sufficient coverage rate in the coal sample. The high ray density with values over 44 at $Z = 50$ mm slice (see Figure 6(b)) guarantees the high *PVT* resolution of imaging damage in the sample core. Additionally, the coal sample under true triaxial loads with $\sigma_1 = 36$ MPa, $\sigma_2 = 18$ MPa, and $\sigma_3 = 16$ MPa had the largest number of AE events during the loading period (2525). The real-time damage characteristics were accurately represented by the six *PVT* cycles with less than 400 AE events, which will be demonstrated in detail in Section 4.2.

3.2. Cumulative AE Energy Density (CAEED). The release of AE energy is a sign of rock fracturing, which are closely related to the damage characteristics and failure intensity of the coal and rocks [34]. Therefore, an index termed *CAEED* was proposed to quantify the energy release level and damage evolution of triaxial loaded coal samples utilizing the energy of AE events. Similar to the *PVT* calculation, the *CAEED* calculation divided the tested coal samples into voxels with dimensions of $5 \times 5 \times 5$ mm. *CAEED* distribution can be extremely concentrated in coal samples due to the full growth of cleats and joints, making it challenging to identify the areas with medium-low *CAEED*. The *CAEED* index adopts a logarithmic function to better visualize the cumulative AE energy features of the tested coal sample. For voxel point *i*, its *CAEED* is derived by using the nearby historical AE events within the radius *R*:

$$\mathrm{CAEED}_i = \sum_{j=1}^{m} 0.5 \ln\left(1 + U_j\right), \tag{4}$$

where m is the number of the historical AE events within the radius R and U_j is the energy of the j^{th} AE events. U_j is in units of attojoule (aJ), which is 10^{-9} joule (J). When determining R, it is important to maximize the use of AE events close to each voxel while minimizing their reuse between the adjacent voxels. In this study, R was determined as the half of the body diagonal of the $5 \times 5 \times 5$ mm voxel, which is 4.3 mm (see Figure 7(a)). Figures 7(b) and 7(c) show an example of the longitudinal sections and cross-sections of the *CAEED* distribution in the triaxial loaded coal sample. A significant amount of *CAEED* was found in the top centre of the sample, whereas only a medium-low level was found in the lower half of the sample. It signifies a significant heterogeneity of the AE energy release of the coal sample under the true triaxial loading.

4. Results

4.1. AE Characteristics of Coal Samples under True Triaxial Loading. Figure 8 shows the results of time-varying stresses and AE events number of coal samples under different true triaxial loading and unloading conditions. The results show that σ_1 of the loaded coal sample reached a value of 71 MPa, which is more than 5 times the coal UCS (13.7 MPa). It implies that the coal strength under true triaxial loading was significantly higher than that under uniaxial loading. The majority of the AE events were detected in all of the coal samples during the loading period, indicating continuous damage caused by the fracturing of the coal. With

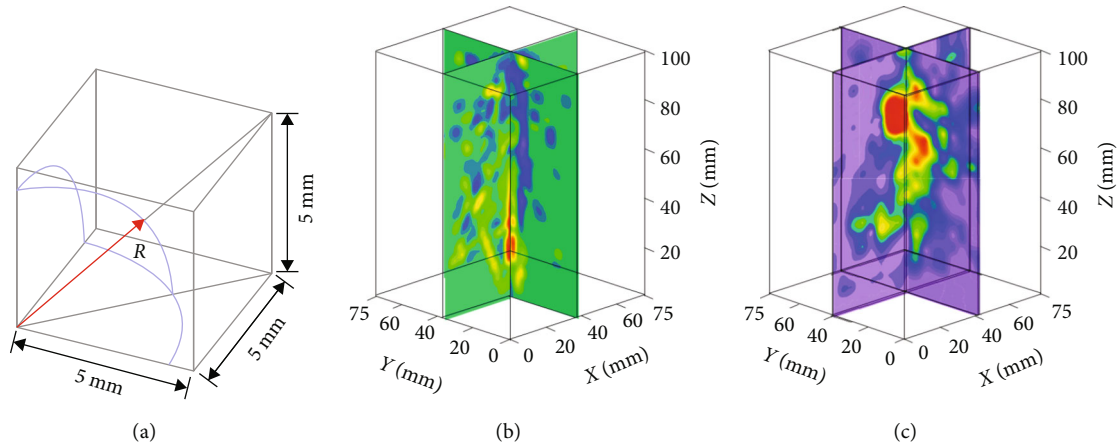

FIGURE 7: (a) R determination: half of the body diagonal of the voxel. (b) Longitudinal sections of *PVT* distribution and (c) *CAEED* distribution in a triaxial loaded coal sample.

the increase of σ_1 levels, the peak number of AE events in the loading process first increased and then decreased. When $\sigma_1 = 26$ MPa and 31 MPa, the peak numbers of AE events in the coal samples were 18 and 17, respectively (see Figures 8(a) and 8(b)). The highest numbers of AE events in the loaded coal samples increased dramatically at $\sigma_1 =$ 36 MPa, 41 MPa, and 46 MPa, to 118, 200, and 170 events, respectively (see Figures 8(c)–8(e)). However, the peak number of AE events decreased to 25 when $\sigma_1 = 71$ MPa (see Figure 8(f)). Such a phenomenon is counterintuitive because an extremely high level of triaxial loading tends to cause more damage to the material. This is evident by the overlap of the frequent AE signals during the test. A high load of $\sigma_1 = 71$ MPa led to the instantaneous formation of lots of fractures. Their AE signals were stacked together, making it difficult to distinguish using the AE monitoring system [35]. During the load holding period, the coal samples with σ_1 no less than 36 MPa presented successive AE events, which indicates the ongoing fractures and damage in the coal (see Figures 8(c)–8(f)). When σ_3 was suddenly released in the dynamic unloading period, the coal samples with σ_1 ranging from 26 to 46 MPa had very few seismic events, with a maximum of 6 AE events during the period (see Figures 8(a)–8(e)). However, the coal sample with $\sigma_1 = 71$ MPa had a dramatic increase of AE events with values of 15, which indicates severe damage and failure due to the sudden σ_3 unloading (see Figure 8(f)).

4.2. Damage Evolution of True Triaxial Loaded Coal Samples. *PVT* and *CAEED* were employed to investigate the damage evolution of the true triaxial loaded coal samples. As discussed in Section 3.1, each *PVT* calculation cycle requires AE events with numbers ranging from 100 to 400 to ensure the timeliness and accuracy of the results. Table 1 lists the number of AE events and *PVT* cycles for triaxial loaded coal samples with different σ_1. Massive seismic data was created by coal samples with σ_1 ranging from 36 to 46 MPa, which contributed 6-9 *PVT* calculating cycles in the loading period and the load holding period. In contrast, because insufficient AE events were detected in the coal samples with σ_1 of 26, 31, and 71 MPa, they presented less than two calculating cycles in the loading period and no calculating cycle in the load holding period. All the tested samples had no *PVT* calculation in the dynamic unloading period as almost no AE signals were detected. To demonstrate the detailed damage evolution characteristics of the triaxial loaded coal, the *PVT* and *CAEED* results of the tested sample with $\sigma_1 = 36$ MPa were analysed in this section, which has 9 calculating cycles (see Figure 9). Adjacent calculating cycles commonly showed similar *PVT* and *CAEED* results; hence, the *PVT* and *CAEED* results for cycles II, IV, VI, and VIII of the tested sample with $\sigma_1 = 36$ MPa were selected to characterise the damage evolution in the coal, which are shown in Figure 10.

Figures 10(a)–10(c) show that there is a large amount of AE activities in the coal sample during the triaxial loading period. Strong AE events with energy larger than 10 k aJ accumulated in the upper half part of the sample, indicating an intensive emergence of fractures. Such damage in the coal sample is also shown as the anomalous wave velocity distributions using *PVT*, which can be seen in Figures 10(e)–10(g). As observed in Figure 10(e), when σ_1 reached 58.4% of the maximum (21/36 MPa), small zones of low velocity with values lower than 1.0 km/s and high velocity with values higher than 1.3 km/s were observed in the upper half part of the sample. This indicates the occurrence of partial stress concentration and fracture emergence in the coal during the initial loading period. When σ_1 reached 84.3% of the maximum (30.3/36 MPa), low velocity zone with values lower than 1.0 km/s expanded along the central longitudinal axis of the sample (see Figure 10(f)). At the same time, the high-velocity zone at the top of the sample with values larger than 1.3 km/s expanded. This implies that successive damage has occurred in the coal during this loading period. The *PVT* result in Figure 10(g) shows that when σ_1 reached 98.8% of the maximum (35.6/36 MPa), many high wave velocity zones appeared along the central longitudinal axis of the sample, where velocities were larger than 1.1 km/s. However, rare low-velocity zones with values smaller than 0.9 km/s were also detected in the sample. This could be due to the

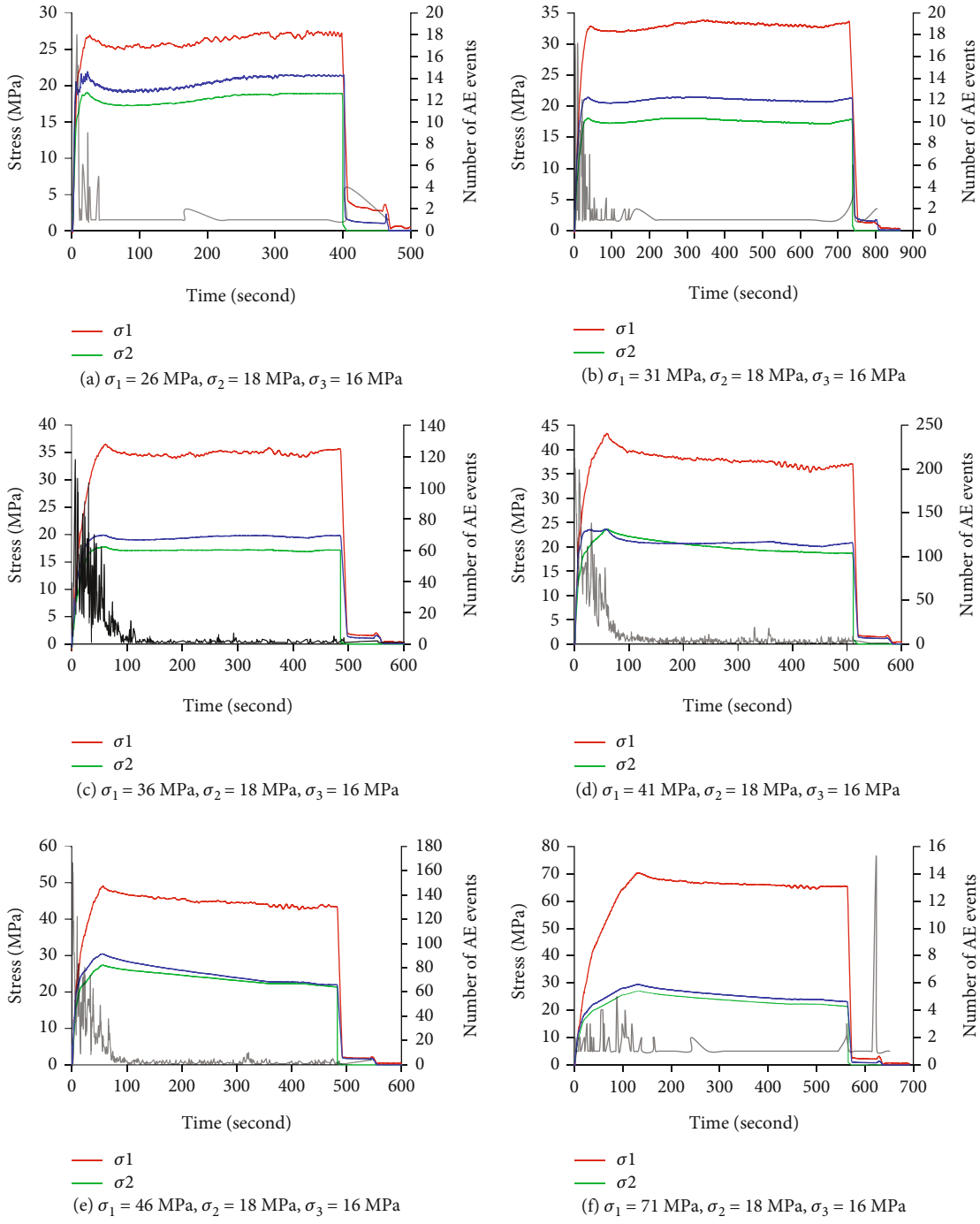

Figure 8: Time-varying stresses and AE event number of coal samples under different true triaxial loading and unloading conditions.

coalescence of fractures caused by the increasing σ_1. During the load holding period, high wave velocity zones with values more than 1.5 km/s migrated from the top to the bottom of the sample, where a higher degree of stress concentration was observed. Low wave velocity zones with values less than 1 km/s enlarged and expanded to the top and mid of the sample, which could have been caused by the continuous emergence of new fractures in the area. Several AE events were still discovered in the coal sample during the load holding time (see Figure 10(d)), and a large area of anomalous velocity zones was found around the axis of the sample (see Figure 10(h)), indicating continuous damage during the period. The *PVT* evolution characteristics prove that many fractures generated in the coal at the initial stage of the triaxial loading, as indicated by the expansion of the low wave velocity area. Due to the high triaxial loads and the accompanying rise in the σ_1 level, the cracks that have occurred had a tendency to consolidate. Partial stress concentration was detected in triaxial loaded coal, which was evident by the appearance of the high wave velocity zones.

Table 1: Number of AE events and *PVT* cycles for triaxial loaded coal samples with different σ_1.

σ_1 of coal samples (MPa)	AE events number during the test	Number of *PVT* cycles during the loading period	Number of *PVT* cycles during the load holding period
26	136	1	0
31	299	2	0
36	3109	6	3
41	4641	6	3
46	3320	5	1
71	166	1	0

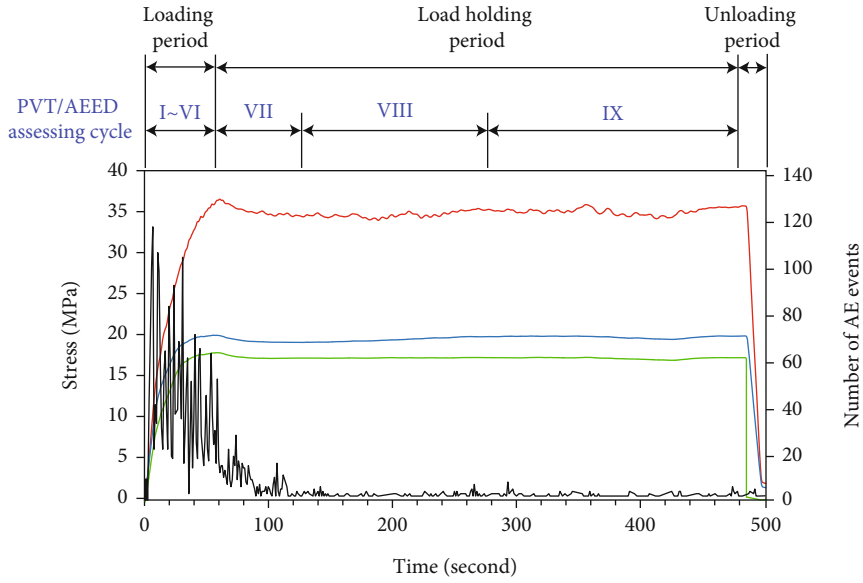

Figure 9: Distribution of *PVT*/*CAEED* calculating cycles for the triaxial loaded coal sample with $\sigma_1 = 36$ MPa, $\sigma_2 = 18$ MPa, and $\sigma_3 = 16$ MPa.

Figures 10(i)–10(k) show the evolution of *CAEED* in the coal sample during the triaxial loading period. It implies that the AE energy was mainly released around the central longitudinal axis, with the maximum *CAEED* value increasing from 16 (see Figure 10(i)) to 26 (see Figure 10(k)). As σ_1 increased, the zones with maximum *CAEED* developed from lower half part to the upper half part of the sample. Continuous coal damage during the load holding time led to an increase in *CAEED* and enlarged *CAEED* zones in the upper half part of the sample, with the maximum *CAEED* reaching up to 30 (see Figure 10(l)). The results in Figures 10(i)–10(l) indicate that intensive energy release in the triaxial loaded coal commonly occurred in the core of the sample, and as the level of triaxial loading increased, the significant energy release zone transferred and expanded.

To investigate the high and low wave velocity characteristics of coal under different triaxial loading conditions, the velocity anomaly index (*VA*) was used to evaluate the degree of the wave velocity anomaly in the tested samples. Each tested coal sample was divided into voxels with dimensions of $5 \times 5 \times 5$ mm for *PVT* and *CAEED* calculation. There were a total of 2000 voxels in a sample. For the i^{th} voxel, its velocity anomaly index $VA_{(i)}$ is calculated as [3]

$$VA_{(i)} = \frac{C_{p(i)} - C_p^a}{C_p^a}, \tag{5}$$

where C_p is the wave velocity of a point in the sample and C_p^a is the average wave velocity in the sample. For high wave velocity zones, a higher *VA* presented more fracture coalescence and/or a higher degree of stress concentration, whereas, for low wave velocity zones, a lower *VA* presented more fracture emergence and/or connections. Figure 11 shows the number of voxels with negative *VA* in the tested samples at the last *PVT* calculating cycle of the triaxial test loading period. For the triaxial loaded coal samples with σ_1 in the range of 26 MPa to 46 MPa, the minimum *VA* increased with the increasing σ_1. The coal samples with σ_1 of 26 MPa and 31 MPa had more negative *VA* voxels than other coal samples, and their minimum *VA* was found to be lower than -0.4. The total number of negative *VA* voxels

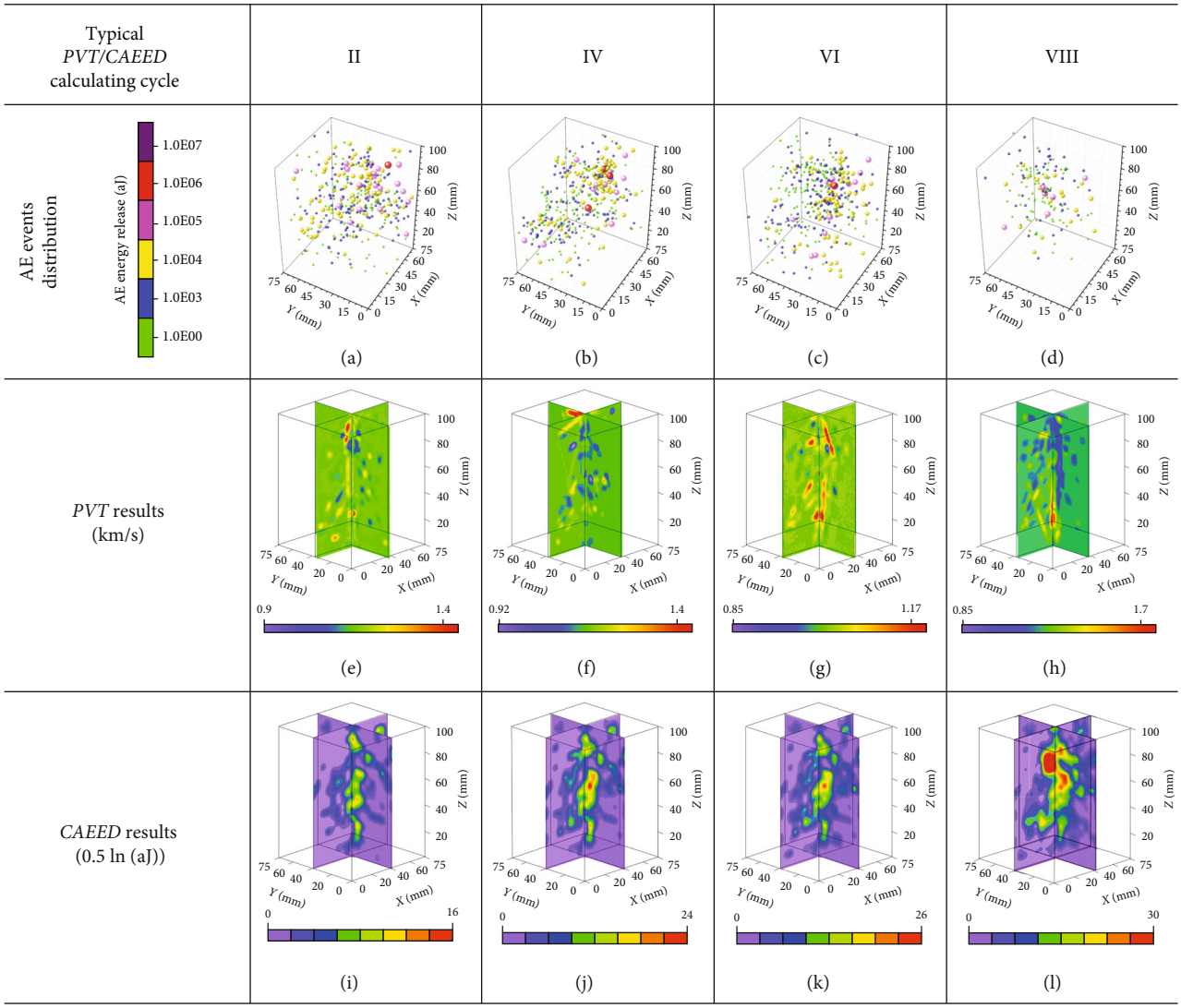

FIGURE 10: Distributions of AE events, *PVT*, and *CAEED* at different calculating cycles for the triaxial loaded coal sample with $\sigma_1 = 36$ MPa, $\sigma_2 = 18$ MPa, and $\sigma_3 = 16$ MPa.

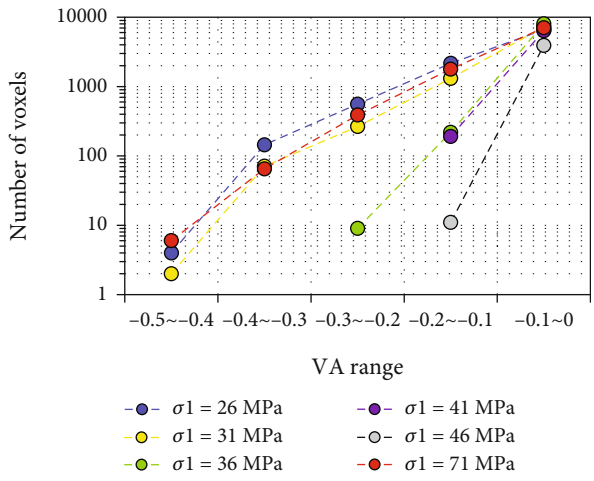

FIGURE 11: Number of voxels with negative velocity anomalies (*VA*) in triaxial loaded coal samples with different σ_1.

decreased for the coal samples with σ_1 from 36 MPa to 46 MPa, while the minimum *VA* increased, ranging from -0.3 to -0.1. Under extremely high triaxial loads of $\sigma_1 = 71$ MPa, the number of negative *VA* voxels in the coal sample showed dramatic increase, and the minimum *VA* was lower than -0.4. The results showed the presence of many pre-existed fractures in the coal, which were unable to coalesce under the lower level of triaxial loads with $\sigma_1 < 31$ MPa. The preexisted fractures started to coalesce when the triaxial loads were between 36 MPa and 46 MPa. This was represented by the decrease in the negative *VA* voxel numbers and an increase in minimum *VA*. The extremely high triaxial loads with $\sigma_1 = 71$ MPa led to significant damage in coal, causing intensive fracture development.

Figure 12 shows the number of voxels with positive *VA* in the tested samples at the last *PVT* calculating cycle during the triaxial test loading period. The coal samples with $\sigma_1 =$ 26 MPa and 31 MPa had more positive *VA* voxels than that present in other coal samples, and their maximum *VA* was

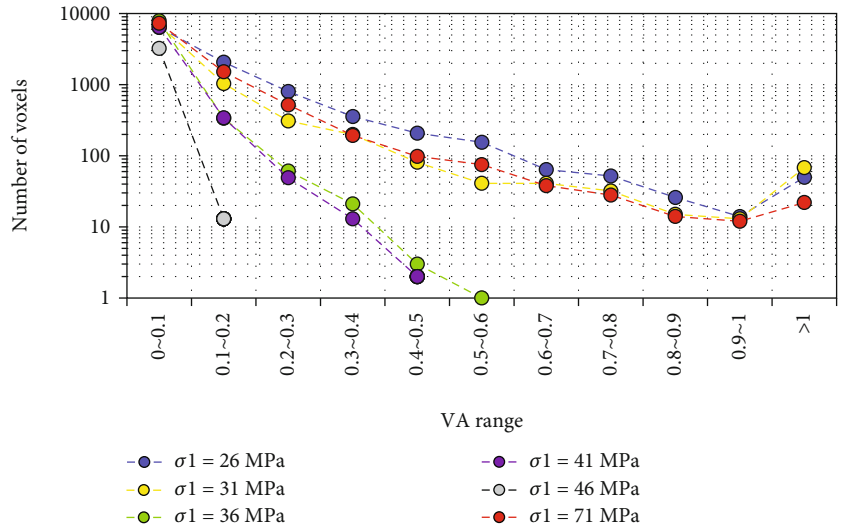

Figure 12: Number of voxels with positive velocity anomalies (*VA*) in triaxial loaded coal samples with different σ_1.

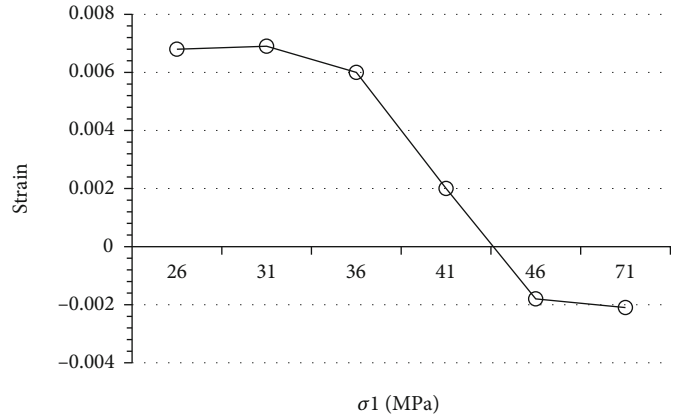

Figure 13: Total strain of coal samples under true triaxial loading with different σ_1.

larger than 1. When σ_1 was between 36 MPa and 41 MPa, the number of positive *VA* voxels decreased significantly, and the maximum *VA* was less than 0.6. A very low velocity anomaly level was observed in the coal sample when σ_1 was 46 MPa. Only a few voxels with *VA* larger than 0.1 were detected, and the maximum *VA* was no more than 0.2. The coal sample under the extremely triaxial stress of $\sigma_1 = 71$ MPa presented a significant number of positive VA voxels, with the maximum VA greater than 1. This was similar to the coal samples under lower levels of triaxial loads (with σ_1 of 26 MPa and 31 MPa). The results in Figure 12 indicate the high VA zones were caused by the high heterogeneity in the coal under lower levels of triaxial loads. When triaxial loads increased, the zones with high density began to undergo damage by generating fractures, which led to a decrease in maximum *VA* values and positive *VA* voxels number. The coal sample under an extremely high level of triaxial loads experienced sufficient damage, but the significant σ_1 contributed to regeneration of high-density zones in the coal, as evidenced by the appearance of massive positive *VA* voxels.

4.3. Damage Mode under True Triaxial Loading and Dynamic Unloading. The total strain of the coal samples with different loading conditions was calculated to explore the deformation characteristics of coal under true triaxial loading and dynamic loading, and the result is given in Figure 13. Total strain, also known as volumetric strain, is the sum of the strains from the three loading directions. When samples are subjected to triaxial stresses with σ_1 less than 41 MPa, a positive total strain was observed, indicating that the crushed coal's size had decreased However, when σ_1 reached 46 MPa, the total strain of the sample became negative, which decreased as σ_1 increased. This phenomenon implies that the strain in the σ_2 and σ_3 directions turned to be negative, and the sum of their absolute values was large than the strain in the σ_1 direction. The true triaxial loads with σ_1 of 46 MPa and 71 MPa contributed to further coal damage, which corresponded to strain-softening conditions. The significant stress deviations ($\sigma_1 - \sigma_2$ and $\sigma_1 - \sigma_3$) led to negative strain with increased absolute values in the σ_2 and σ_3 directions.

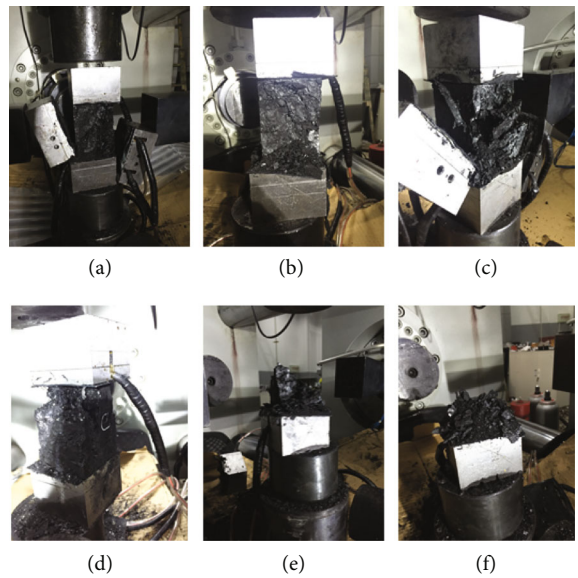

Figure 14: Failure mode of coal samples after true triaxial loading and dynamic unloading tests with different σ_1. (a) $\sigma_1 = 26$ MPa, (b) $\sigma_1 = 31$ MPa, (c) $\sigma_1 = 36$ MPa, (d) $\sigma_1 = 41$ MPa, (e) $\sigma_1 = 46$ MPa, (f) $\sigma_1 = 71$ MPa.

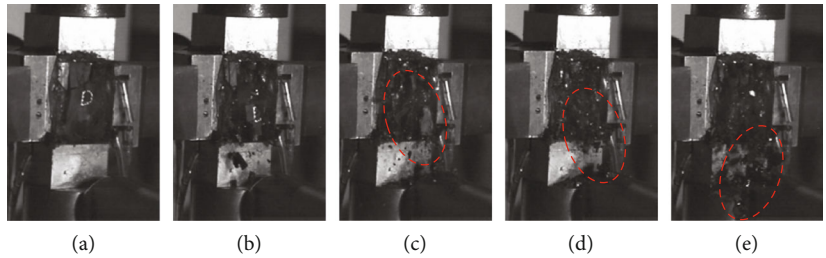

Figure 15: Dynamic failure moment of the triaxial loaded coal sample ($\sigma_1 = 71$ MPa, $\sigma_2 = 18$ MPa, and $\sigma_3 = 16$ MPa) when suddenly releasing σ_3 by dropping the loading bar in the horizontal direction. The red ellipse marks the ejected coal fragments from the coal sample.

Figure 14 shows the failure mode of coal samples after true triaxial loading and dynamic unloading tests. When $\sigma_1 = 26$ MPa, the coal sample remained intact, and no visible fragments detached from the body (Figure 14(a)). When $\sigma_1 = 31$ MPa, a small amount of coal fragments was found to be falling from the lower boundary of the sample (Figure 14(b)). It implies that the triaxial loads and dynamic unloads caused partial damage in the coal sample. When $\sigma_1 = 36$ MPa, flaky coal fragments was found on one side of the sample (Figure 14(c)). Such phenomenon can be illustrated by the fractures development along with the internal fissures of the coal sample, i.e., cleats and joints. When $\sigma_1 = 41$ MPa, the coal on the edge of the sample was split, but the major part of the sample remained intact (Figure 14(d)). At $\sigma_1 = 46$ MPa, the sample failed along with the formation of internal fissures in the coal, and only a few parts of the coal were found on the bottom loading plate, suggesting that such a triaxial loading caused the failure of the coal sample (Figure 14(e)). When σ_1 was further increased to 71 MPa, the coal sample failed and was severely damaged. Only a few coal fragments were left on the bottom loading plate. It demonstrates that under such significantly high σ_1 and stress deviation, even the internal fissures of the coal were sufficiently damaged, contributing to a complete loss of the bearing capacity.

Figure 15 shows the dynamic failure instance of the triaxial loaded coal sample ($\sigma_1 = 71$ MPa, $\sigma_2 = 18$ MPa, and $\sigma_3 = 16$ MPa), captured by the high-speed camera, when σ_3 was suddenly released by dropping the loading bar in the horizontal direction. In Figure 15(a), the exposed coal surface was initially complete due to the holding of the droppable loading plate. Following that, a large number of coal fragments erupted from the coal sample (see Figures 15(b)–15(e)). Most of the coal fragments were in small sizes, and their ejected velocities were typically low. It confirms that the coal sample under an extremely high level of true triaxial loading failed and was sufficiently damaged. Therefore, the coal had almost no bearing capacity or the stored strain energy inside, which led to low-velocity ejections of the coal fragments.

5. Conclusions

The in situ stress and complex loading-unloading paths are closely associated with the coal burst proneness. To better understand the damage and failure characteristics of coal

under mining conditions, the self-developed multifunctional coal burst testing system, TTCDBTS, was used to reproduce in situ triaxial loading and dynamic unloading of the coal sample in the laboratory. Six coal samples were tested under true triaxial loads with σ_1 ranging from 26 MPa to 71 MPa, σ_2 of 18 MPa, and σ_3 of 16 MPa. Each sample experienced the true triaxial loading test period, the loading holding period, and the dynamic unloading test period. The coal strength under actual triaxial loading was found to be more than 5 times more than the UCS. The results of AE monitoring during the tests indicated that continuous coal damage mainly occurred during the true triaxial loading test period. The peak AE event number in the tested samples first increased and then decreased as σ_1 levels increased. *PVT* and *CAEED* were used to analyse the stress and damage evolution characteristics of the coal. The *PVT* results demonstrated that the fracture emergence at the initial loading stage could be presented by the expansion of the low wave velocity area. The increasing σ_1 level caused fracture coalescence and regenerations of high-density zones in the coal, which was identified by the high wave velocity area. The total strain of the coal samples was found to be negative under significant stress deviations. Under an extremely high level of triaxial loads, the coal samples failed and were severely damaged. Ejection of coal fragments occurred at low velocities when σ_3 was dynamically unloaded. The outcome of this study can help in understanding the dynamic failure mechanism of the coal mass when developing roadways near the geological are typical.

Data Availability

The data used in this work are from Huating Coal Mine, and they are confidential.

Conflicts of Interest

The authors declared that they have no conflicts of interest in this work.

Acknowledgments

This research is supported by the Foundation of China under Grant Nos. U21A20110 and 51734009 and the Major Science and Technology Innovation Program of Shandong Province under Grant No. 2019SDZY02.

References

[1] N. G. W. Cook, "A note on rockbursts considered as a problem of stability," *Journal of the Southern African Institute of Mining and Metallurgy*, vol. 65, no. 8, pp. 437–446, 1965.

[2] C. Zhang, I. Canbulat, B. Hebblewhite, and C. R. Ward, "Assessing coal burst phenomena in mining and insights into directions for future research," *International Journal of Coal Geology*, vol. 179, pp. 28–44, 2017.

[3] A. Cao, L. Dou, C. Wang, X. X. Yao, J. Y. Dong, and Y. Gu, "Microseismic precursory characteristics of rock burst hazard in mining areas near a large residual coal pillar: a case study from Xuzhuang Coal Mine, Xuzhou, China," *Rock Mechanics and Rock Engineering*, vol. 49, no. 11, pp. 4407–4422, 2016.

[4] A. Cao, L. Dou, W. Cai, S. Gong, S. Liu, and G. Jing, "Case study of seismic hazard assessment in underground coal mining using passive tomography," *International Journal of Rock Mechanics and Mining Sciences*, vol. 78, pp. 1–9, 2015.

[5] Y. Jiang, Y. Pan, F. Jiang, L.-M. Dou, and Y. Ju, "State of the art review on mechanism and prevention of coal bumps in China," *Journal of China Coal Society*, vol. 39, no. 2, pp. 205–213, 2014.

[6] A. T. Iannacchione and S. C. Tadolini, "Occurrence, predication, and control of coal burst events in the US," *International Journal of Mining Science Technology*, vol. 26, no. 1, pp. 39–46, 2016.

[7] R. Patyńska, A. Mirek, Z. Burtan, and E. Pilecka, "Rockburst of parameters causing mining disasters in mines of Upper Silesian Coal Basin," *E3S Web of Conferences*, vol. 36, article 03005, 2018.

[8] W. Ortlepp, "RaSiM comes of age—a review of the contribution to the understanding and control of mine rockbursts," in *Proceedings of the Sixth International Symposium on Rockburst and Seismicity in Mines Proceedings*, pp. 3–20, Perth, Western Australia, 2005.

[9] A. Jager and J. Ryder, *A handbook on rock engineering practice for tabular hard rock mines*, Safety in Mines Research Advisory Committee, Johannesburg, 1999.

[10] M. Cai, "Influence of intermediate principal stress on rock fracturing and strength near excavation boundaries–Insight from numerical modeling," *International Journal of Rock Mechanics and Mining Sciences*, vol. 45, no. 5, pp. 763–772, 2008.

[11] J. Li, J. Zhao, S. Gong et al., "Mechanical anisotropy of coal under coupled biaxial static and dynamic loads," *International Journal of Rock Mechanics and Mining Sciences*, vol. 143, article 104807, 2021.

[12] S. D. Goodfellow, *Quantitative analysis of acoustic emission from rock fracture experiments*, University of Toronto (Canada), 2015.

[13] G. Su, Y. Shi, X. Feng, J. Jiang, J. Zhang, and Q. Jiang, "True-triaxial experimental study of the evolutionary features of the acoustic emissions and sounds of rockburst processes," *Rock Mechanics and Rock Engineering*, vol. 51, no. 2, pp. 375–389, 2018.

[14] B. Haimson and C. Chang, "A new true triaxial cell for testing mechanical properties of rock, and its use to determine rock strength and deformability of Westerly granite," *International Journal of Rock Mechanics and Mining Sciences*, vol. 37, no. 1-2, pp. 285–296, 2000.

[15] P.-Z. Pan, X.-T. Feng, and J. Hudson, "The influence of the intermediate principal stress on rock failure behaviour: a numerical study," *Engineering Geology*, vol. 124, pp. 109–118, 2012.

[16] M. Tibbo, *A true-triaxial laboratory seismic velocity experiment under in situ stress conditions: a comparison with in situ 3D stress and velocity*, University of Toronto (Canada), 2018.

[17] K. Mogi, "Fracture and flow of rocks under high triaxial compression," *Journal of Geophysical Research*, vol. 76, no. 5, pp. 1255–1269, 1971.

[18] A. M. Al-Ajmi and R. W. Zimmerman, "Relation between the Mogi and the Coulomb failure criteria," *International Journal*

of Rock Mechanics and Mining Sciences, vol. 42, no. 3, pp. 431–439, 2005.

[19] L. R. Alejano and A. Bobet, "Drucker–prager criterion," in *The ISRM Suggested Methods for Rock Characterization, Testing and Monitoring: 2007-2014*, R. Ulusay, Ed., pp. 247–252, Springer, Cham, 2012.

[20] J. Galvin, *Ground Engineering - Principles and Practices for Underground Coal Mining*, Springer, 2016.

[21] J. Lu, G. Yin, D. Zhang, H. Gao, C. Li, and M. Li, "True triaxial strength and failure characteristics of cubic coal and sandstone under different loading paths," *International Journal of Rock Mechanics and Mining Sciences*, vol. 135, article 104439, 2020.

[22] J. Zhang, C. Ai, Y.-W. Li et al., "Energy-based brittleness index and acoustic emission characteristics of anisotropic coal under triaxial stress condition," *Rock Mechanics and Rock Engineering*, vol. 51, no. 11, pp. 3343–3360, 2018.

[23] Y. Liu, G. Yin, M. Li et al., "Anisotropic mechanical properties and the permeability evolution of cubic coal under true triaxial stress paths," *Rock Mechanics and Rock Engineering*, vol. 52, no. 8, pp. 2505–2521, 2019.

[24] A. Alexeev, V. Revva, N. Alyshev, and D. M. Zhitlyonok, "True triaxial loading apparatus and its application to coal outburst prediction," *International Journal of Coal Geology*, vol. 58, no. 4, pp. 245–250, 2004.

[25] Q. Zhang and J. Zhao, "A review of dynamic experimental techniques and mechanical behaviour of rock materials," *Rock Mechanics and Rock Engineering*, vol. 47, no. 4, pp. 1411–1478, 2014.

[26] X.-T. Feng, Y. Gao, X. Zhang, Z. Wang, Y. Zhang, and Q. Han, "Evolution of the mechanical and strength parameters of hard rocks in the true triaxial cyclic loading and unloading tests," *International Journal of Rock Mechanics and Mining Sciences*, vol. 131, article 104349, 2020.

[27] X. Zhao, J. Wang, M. Cai et al., "Influence of unloading rate on the strainburst characteristics of Beishan granite under true-triaxial unloading conditions," *Rock Mechanics and Rock Engineering*, vol. 47, no. 2, pp. 467–483, 2014.

[28] M. He, J. Li, D. Liu, and J. Sun, "Latest Progress of Research on Rockburst Experiment Mechanism and Its Control," *IOP Conference Series: Earth and Environmental Science*, no. article 032033, 2020.

[29] M. He, J. Miao, and J. Feng, "Rock burst process of limestone and its acoustic emission characteristics under true-triaxial unloading conditions," *International Journal of Rock Mechanics and Mining Sciences*, vol. 47, no. 2, pp. 286–298, 2010.

[30] J. Li, H. Wang, and Q. Zhang, "Progressive damage and fracture of biaxially-confined anisotropic coal under repeated impact loads," *International Journal of Rock Mechanics and Mining Sciences*, vol. 149, article 104979, 2022.

[31] C. Wang, "Evolution characters of stress and energy and laws of fractures and damage in coal sample under true tri-axial loading-unloading test," China University of Mining and Technology, 2017.

[32] J. Bai, W. Shen, G. Guo, X. Y. Wang, and Y. Yu, "Roof deformation, failure characteristics, and preventive techniques of gob-side entry driving heading adjacent to the advancing working face," *Rock Mechanics and Rock Engineering*, vol. 48, no. 6, pp. 2447–2458, 2015.

[33] N. Hosseini, K. Oraee, K. Shahriar, and K. Goshtasbi, "Passive seismic velocity tomography on longwall mining panel based on simultaneous iterative reconstructive technique (SIRT)," *Journal of Central South University*, vol. 19, no. 8, pp. 2297–2306, 2012.

[34] S. J. Gibowicz and A. Kijko, *An Introduction to Mining Seismology*, Polish Academy of Sciences, Warsaw, Poland, 1994.

[35] J. Li, *Mechanical and Microseismic Characteristics of Anisotropic Coal under Static and Dynamic Loads*, Monash University, 2021.